Effect of Turnaround Lines of Magnetic Flux in Two-Dimensional MHD Channel Flow under a Traveling Sine Wave Magnetic Field

doi: 10.1063/1.858871

Effect of turnaround lines of magnetic flux in two-dimensional MHD channel flow under a traveling sine wave magnetic field

Kazuyuki Ueno
Department of Aeronautical Engineering, Kyoto University, Kyoto 606, Japan

(Received 14 April 1992; accepted 29 September 1992)

Laminar liquid metal flow fields between two parallel insulator walls under a traveling sine wave magnetic field are numerically solved for a small magnetic Reynolds number. When both average Hartmann number H_a and cubic root of interaction parameter $N^{1/3}$ are much greater than dimensionless wavelength Λ, a set of turnaround lines of magnetic flux, which exist every half-wavelength, cause a set of recirculating flows. Consequently a nozzlelike converging and diverging flow is formed between them. The throat width of the nozzlelike flow is estimated to be the greater of $N^{-1/4}\Lambda^{3/4}$ or $H_a^{-1/2}\Lambda^{1/2}$ compared with the channel height.

I. INTRODUCTION

The flow field of an electrically conducting incompressible viscous fluid between two parallel insulator walls is affected (i) by inertia, (ii) by the two-dimensionality of the imposed magnetic field, and (iii) by the induced magnetic field under a traveling sine wave transverse magnetic field. In a previous paper,[1] the inertia effect on laminar flows was clarified. In this paper, the effect of the two-dimensionality of the imposed magnetic field on laminar flows is examined under an assumption of a negligibly small effect of the induced magnetic field.

II. GOVERNING EQUATIONS

We carry out the analyses on the coordinate system moving with the traveling magnetic field. In this coordinate system, we can assume the magnetic and flow fields to be steady and the electric field to be negligible for the infinitely extended two-dimensional channel.[1]

Figure 1 shows the flow configuration and typical lines of magnetic flux; the magnetic flux density for a small magnetic Reynolds number is

$$B_x=\cos x\,\frac{\sinh(\Lambda^{-1}y)}{\Lambda\cosh\Lambda^{-1}},\quad B_y=\sin x\,\frac{\cosh(\Lambda^{-1}y)}{\cosh\Lambda^{-1}} \tag{1}$$

in the dimensionless form.[1] The two-dimensionality of the imposed magnetic field causes the turnaround lines of magnetic flux in $\sin^2 x \leqslant \tanh^2(\Lambda^{-1}y)$.

The dimensionless governing equations[1] are

$$\frac{\partial u}{\partial x}+\frac{\partial v}{\partial y}=0, \tag{2}$$

$$\frac{1}{N}\left(u\frac{\partial u}{\partial x}+v\frac{\partial u}{\partial y}\right)=-\frac{\partial p}{\partial x}+\frac{\Delta u}{H_a^2}-2(uB_y-vB_x)B_y, \tag{3}$$

$$\frac{1}{N\Lambda^2}\left(u\frac{\partial v}{\partial x}+v\frac{\partial v}{\partial y}\right)=-\frac{\partial p}{\partial y}+\frac{\Delta v}{H_a^2\Lambda^2}+2(uB_y-vB_x)B_x, \tag{4}$$

where $\Delta=\Lambda^{-2}\partial^2/\partial x^2+\partial^2/\partial y^2$. The flow velocity (u,v) and the pressure gradient $\partial p/\partial x$ are periodic functions of x. The average pressure gradient, which drives the fluid, is $\langle\partial p/\partial x\rangle_{av}=-1$. The boundary conditions $u=-S$ and $v=0$ are required at the walls $y=\pm 1$.

The dimensionless parameters in Eqs. (1)–(4) are defined with $\Lambda=\lambda/(2\pi h)$, $H_a=(\sigma_L/2\eta_L)^{1/2}hB_0$, $N=(\sigma_L\lambda B_0^2)/(4\pi\rho_L U_0)$, and $S=U_s/U_0$; where λ, $2h$, B_0, U_0, and U_s denote the wavelength, the channel height, the amplitude of the sine wave magnetic field, the characteristic flow velocity, and the phase velocity of the traveling magnetic field, respectively; the density ρ_L, the viscosity η_L, and the electric conductivity σ_L of the fluid are assumed to be constant. Average Hartmann number H_a, interaction parameter N, and dimensionless wavelength Λ characterize the effects of viscosity, inertia, and the two-dimensionality of the imposed magnetic field, respectively. We consider the cases limited to $H_a \geqslant 10$, $N \geqslant 10$, and $\Lambda^2 \geqslant 10$.

III. RESULTS AND DISCUSSION

Equations (2)–(4) were numerically solved by using the marker-and-cell (MAC) method.[2] The steady solution was obtained as a converged solution to a time-dependent initial value problem. The Euler backward scheme was adopted. A 100×100 irregular rectangular staggered mesh system was employed.

In the bulk flow and its boundary layer, all the numerical solutions agree with the following analytical solution[1] for large Λ, large N, and a small magnetic Reynolds number to a good approximation:

$$u=\Psi-(\Psi+S)\,\frac{H_l\cosh H_l y-\sinh H_l}{H_l\cosh H_l-\sinh H_l}, \tag{5}$$

where 2Ψ is the flow rate and $H_l=\sqrt{2}H_a\sin x$.

On the other hand, in the thin transverse regions containing the plane $x=k\pi$ (k being an integer), the velocity distribution changes remarkably with Λ and N. We call this region "the nodal region," where $\partial u/\partial x$ is much larger than in the bulk flow. The flows in the nodal region can be classified into three types: (i) the viscous type, (ii) the inertia type, and (iii) the nozzle type. Equation (5) represents the velocity distribution in the viscous type nodal region $H_l \lesssim 1$. The flow field in the inertia type nodal re-

 0899-8213/93/020490-03$06.00

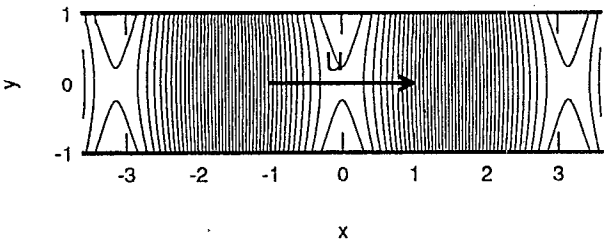

FIG. 1. Flow configuration and lines of magnetic flux; $\Lambda=3.162$.

gion, which has been discussed in the previous paper,[1] is also independent of Λ. The effect of the two-dimensionality of the imposed magnetic field is remarkable in the nozzle-type nodal region.

Streamlines of a typical numerical solution in the nozzle-type nodal region are shown with lines of magnetic flux in Fig. 2. A set of turnaround lines of magnetic flux cause a set of recirculating flows; consequently a nozzlelike converging and diverging flow is formed between them.

The classification of the flows in the nodal region is definitely explained by the asymptotic behavior of the momentum equations for large Λ, H_a, and N.

The thickness of the nodal region in the x direction is denoted by ϵ. By using ϵ ($\ll 1$), each parameter is replaced and the stretched coordinates are introduced as follows:

$$\Lambda=\epsilon^{-l},\quad H_a=\epsilon^{-m},\quad N=\epsilon^{-n};\quad x=\epsilon\tilde{x},\quad y=\tilde{y}. \tag{6}$$

Variables $\tilde{u}=u$, $\tilde{v}=\epsilon v$, $\tilde{p}=\epsilon^{-3}p$, $\tilde{B}_x=\epsilon^{-2l}B_x$, and $\tilde{B}_y=\epsilon^{-1}B_y$ are expected to be $O(1)$ functions of $\tilde{x}$ and $\tilde{y}$. Substituting Eqs. (6) into Eqs. (2)–(4), we obtain the equations for the nodal region.

Only three kinds of force balances are possible. In the cases of (i) $m=1$, $n>3$, $l>1$, (ii) $n=3$, $m>1$, $l>1$, and (iii) $l=1$, $m>1$, $n>3$, the momentum equations are reduced to

$$0=-\frac{\partial\tilde{p}}{\partial\tilde{x}}+\frac{\partial^2\tilde{u}}{\partial\tilde{y}^2}-2\tilde{u}\tilde{B}_y^2,$$
$$0=-\frac{\partial\tilde{p}}{\partial\tilde{y}}, \tag{7}$$
$$\tilde{u}\frac{\partial\tilde{u}}{\partial\tilde{x}}+\tilde{v}\frac{\partial\tilde{u}}{\partial\tilde{y}}=-\frac{\partial\tilde{p}}{\partial\tilde{x}}-2\tilde{u}\tilde{B}_y^2,$$
$$0=-\frac{\partial\tilde{p}}{\partial\tilde{y}}, \tag{8}$$
$$0=-\frac{\partial\tilde{p}}{\partial\tilde{x}}-2(\tilde{u}\tilde{B}_y-\tilde{v}\tilde{B}_x)\tilde{B}_y,$$
$$0=-\frac{\partial\tilde{p}}{\partial\tilde{y}}+2(\tilde{u}\tilde{B}_y-\tilde{v}\tilde{B}_x)\tilde{B}_x, \tag{9}$$

respectively, where we neglect small-order terms. Equations (7)–(9) show the force balance in the viscous-type nodal region, the inertia-type nodal region, and the nozzle-type nodal region, respectively. According to the above analysis, the conditions and the thickness of the nodal region ϵ are estimated as shown in Table I. No solution to our numerical calculations contradicts these estimations.

TABLE I. Analytical estimations of the conditions and the thickness of the nodal region ϵ.

Type	Conditions	ϵ
Viscous type	$1\ll H_a\ll N^{1/3}$, $1\ll H_a\ll\Lambda$	$O(H_a^{-1})$
Inertia type	$1\ll N^{1/3}\ll H_a$, $1\ll N^{1/3}\ll\Lambda$	$O(N^{-1/3})$
Nozzle type	$1\ll\Lambda\ll H_a$, $1\ll\Lambda\ll N^{1/3}$	$O(\Lambda^{-1})$

The magnetic flux density is $\tilde{B}_x=\tilde{y}$, $\tilde{B}_y=\tilde{x}$ for large Λ. For this magnetic field, there is an weak solution of Eq. (9):

$$\tilde{u}=\Psi\,\mathrm{sgn}(\tilde{x})\frac{\partial\tilde{g}}{\partial\tilde{y}},\quad \tilde{v}=-\Psi\,\mathrm{sgn}(\tilde{x})\frac{\partial\tilde{g}}{\partial\tilde{x}}, \tag{10}$$

for $\tilde{y}^2\leqslant\tilde{x}^2$, and $\tilde{u}=0$, $\tilde{v}=0$ for $\tilde{y}^2>\tilde{x}^2$, where

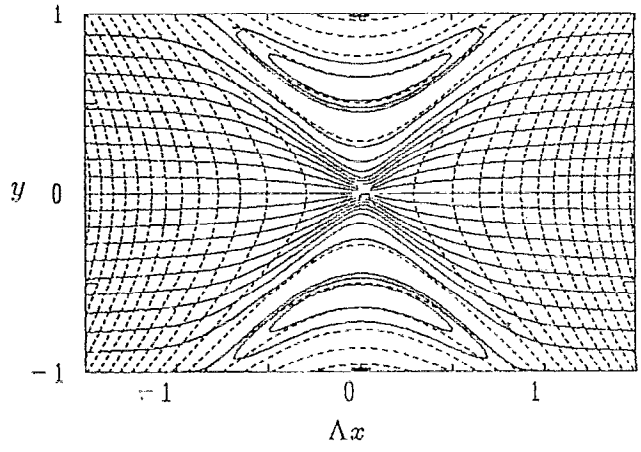

FIG. 2. Streamlines (solid) and lines of magnetic flux (dashed) of a numerical solution in the nozzle-type nodal region; $\Lambda=3.162$, $H_a=3.162\times10^3$, $N=10^6$, $S=1$.

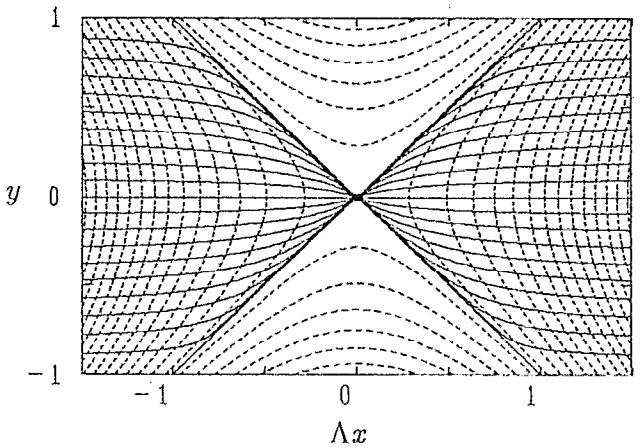

FIG. 3. Streamlines (solid) and lines of magnetic flux (dashed) of the analytical solution in the nozzle-type nodal region.

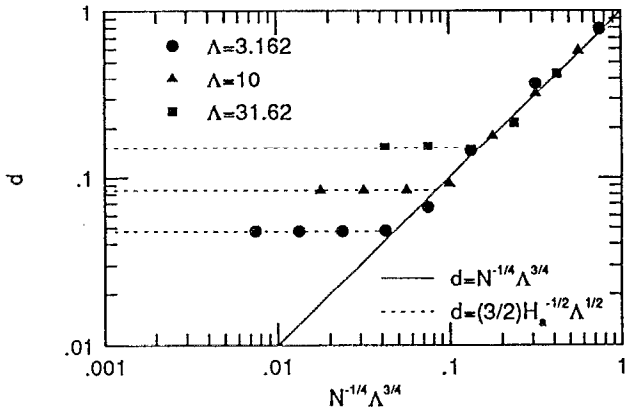

FIG. 4. Numerical results of the half-width of the throat d; $H_a=3.162\times10^3$, $S=1$.

$$\tilde{g}(\tilde{x},\tilde{y})=\frac{\log|\tilde{x}+\tilde{y}|-\log|\tilde{x}-\tilde{y}|}{2\log(1+\sqrt{\tilde{x}^2-\tilde{y}^2+1})-\log(\tilde{x}^2-\tilde{y}^2)}.$$

Figure 3 shows the streamlines of the above solution with the lines of magnetic flux. A set of recirculating flows from the numerical solution reduce to a set of stagnant fluid regions. This result shows (i) that the asymptotic analysis successfully represents the force balance in the nodal region, and (ii) that the nozzle-type nodal region has fine structures on $\tilde{y}=\pm\tilde{x}$ and $\tilde{y}=\pm1$, where the simplified equation (9) is not appropriate.

We are interested in the fine structure which contains the point of the largest flow velocity in the nozzle-type nodal region; we call this fine structure "the throat" after ordinary nozzle flow.

In the cross section of the largest velocity point, there are four inflection points where $\partial^2\tilde{u}/\partial\tilde{y}^2=0$; the outer two points exist in the recirculating flow and the inner two points exist on the border of the nozzlelike flow. We define the throat width $2d$ to be the distance between the inner two points. Figure 4 shows d's of the numerical solutions. The half-width d is nearly equal to $N^{-1/4}\Lambda^{3/4}$, though d has an lower limit nearly equal to $\frac{3}{2}H_a^{-1/2}\Lambda^{1/2}$.

The results in Fig. 4 can be explained by the asymptotic behavior of the momentum equations; the following procedure is the same as Eqs. (6)–(9).

TABLE II. Analytical estimations of the conditions and the half-width of the throat d for each widening force.

Widening force	Conditions	d
Viscous force	$1\ll\Lambda^3\ll H_a^2\Lambda\ll N$	$O(H_a^{-1/2}\Lambda^{1/2})$
Inertia force	$1\ll\Lambda^3\ll N\ll H_a^2\Lambda$	$O(N^{-1/4}\Lambda^{3/4})$

By using $d(\ll1)$, the parameters are replaced and further stretched coordinates are introduced as follows:

$$\Lambda^2/H_a^2=d^m,\quad \Lambda^3/N=d^n;\quad \tilde{x}=d\hat{x},\quad \tilde{y}=d\hat{y}. \tag{11}$$

Variables $\hat{u}=d\tilde{u}$, $\hat{v}=d\tilde{v}$, $\hat{p}=d^{-2}\tilde{p}$, $\hat{B}_x=d^{-1}\tilde{B}_x$, and $\hat{B}_y=d^{-1}\tilde{B}_y$ are expected to be $O(1)$ functions of $\hat{x}$ and $\hat{y}$. Substituting Eqs. (11) into Eqs. (2)–(4), we obtain the equations for the throat.

Only two kinds of force balances are possible. In the cases of (i) $m=4$, $n>4$ and (ii) $n=4$, $m>4$, the momentum equations are reduced to

$$\begin{aligned}
0&=-\frac{\partial\hat{p}}{\partial\hat{x}}+\frac{\partial^2\hat{u}}{\partial\hat{x}^2}+\frac{\partial^2\hat{u}}{\partial\hat{y}^2}-2(\hat{u}\hat{B}_y-\hat{v}\hat{B}_x)\hat{B}_y,\\
0&=-\frac{\partial\hat{p}}{\partial\hat{y}}+\frac{\partial^2\hat{v}}{\partial\hat{x}^2}+\frac{\partial^2\hat{v}}{\partial\hat{y}^2}+2(\hat{u}\hat{B}_y-\hat{v}\hat{B}_x)\hat{B}_x,
\end{aligned} \tag{12}$$

$$\begin{aligned}
\hat{u}\frac{\partial\hat{u}}{\partial\hat{x}}+\hat{v}\frac{\partial\hat{u}}{\partial\hat{y}}&=-\frac{\partial\hat{p}}{\partial\hat{x}}-2(\hat{u}\hat{B}_y-\hat{v}\hat{B}_x)\hat{B}_y,\\
\hat{u}\frac{\partial\hat{v}}{\partial\hat{x}}+\hat{v}\frac{\partial\hat{v}}{\partial\hat{y}}&=-\frac{\partial\hat{p}}{\partial\hat{y}}+2(\hat{u}\hat{B}_y-\hat{v}\hat{B}_x)\hat{B}_x,
\end{aligned} \tag{13}$$

respectively, where we neglect small-order terms. The above equations show that either the viscous force or the inertia force widens the throat to finite width. According to the above analysis, the conditions and the half-width of the throat d for each widening force are estimated as shown in Table II. The results in Table II agree with the numerical results in Fig. 4.

ACKNOWLEDGMENTS

I would like to thank Professor Shigeki Morioka and Professor Ryuji Ishii for their helpful advice. I also acknowledge valuable discussions with Hirotaka Muraki.

[1] K. Ueno, "Inertia effect in two-dimensional MHD channel flow under a traveling sine wave magnetic field," Phys. Fluids A **3**, 3107 (1991).
[2] F. H. Harlow and J. E. Welch, "Numerical calculation of time-dependent viscous incompressible flow of fluid with free surface," Phys. Fluids **8**, 2182 (1965).